Nanoscale

COMMUNICATION

View Article Online
View Journal

Cite this: DOI: 10.1039/c5nr06727h

Received 29th September 2015,
Accepted 27th January 2016

DOI: 10.1039/c5nr06727h

www.rsc.org/nanoscale

Ultrasensitive 1D field-effect phototransistors: $CH_3NH_3PbI_3$ nanowire sensitized individual carbon nanotubes†

M. Spina,[a] B. Náfrádi,*[a] H. M. Tóháti,[b] K. Kamarás,[b] E. Bonvin,[a] R. Gaal,[a] L. Forró[a] and E. Horváth[a]

Field-effect phototransistors were fabricated based on individual carbon nanotubes (CNTs) sensitized by $CH_3NH_3PbI_3$ nanowires ($MAPbI_3$NWs). These devices represent light responsivities of R = 7.7 × 10^5 A W^{-1} under low-lighting conditions in the nW mm^{-2} range, unprecedented among CNT-based photodetectors. At high incident power (~1 mW mm^{-2}), light soaking results in a negative photocurrent, turning the device insulating. We interpret the phenomenon as a result of efficient free photoexcited charge generation and charge transfer of photoexcited holes from the perovskite to the carbon nanotube. The charge transfer improves conductance by increasing the number of carriers, but leaves electrons behind. At high illumination intensity their random electrostatic potential quenches mobility in the nanotube.

In various optoelectronic applications, like light-emitting diodes, photodetectors and photovoltaic cells, semiconducting carbon nanotubes (CNTs) have been successfully used due to their direct band gap and outstanding electronic and mechanical properties.[1] Photodetection of individual CNTs excited by infrared[2–4] (IR) or visible light[5] has been achieved by separating the excitons with large enough electric fields generated locally by asymmetric Schottky contacts,[2] p–n junctions[3] or local charge defects.[5] However, their performance has been limited to quantum efficiencies of about 10%.[4] This is mainly limited by the high binding energy and long lifetime of excitons in CNTs.[1,6]

$CH_3NH_3PbI_3$ ($MAPbI_3$) is efficiently used as a photosensitizer in many optoelectronic hybrid devices in conjunction with carbon nanomaterials, due to its exceptional, but still not completely explained, physical properties favorable for light harvesting (*i.e.* direct bandgap, large absorption coefficient, long charge diffusion lengths), chemical flexibility and low-cost solution-based processability.[7–10] Several types of heterostructures have been made by combining $MAPbI_3$ and different carbon materials. Fullerenes have been reported to enhance the stability and to reduce drifts and hysteretic effects of $MAPbI_3$ solar cells.[11,12] Incorporation of graphene and carbon nanotube films resulted in semitransparent flexible solar cells.[13,14] The graphene lead–halide interface as a hybrid phototransistor was used as a high-sensitivity phototransistor owing to the successful photo-gating of graphene.[15–17]

Here we studied the light induced transfer characteristics of micro-fabricated field-effect transistors, built from individual metallic and semiconducting CNTs and $CH_3NH_3PbI_3$ nanowires (hereafter $MAPbI_3$NWs). The sensitization of individual CNT-FETs with a network of $MAPbI_3$ nanowires resulted in responsivities as high as 7.7 × 10^5 A W^{-1} and external quantum efficiencies of 1.5 × 10^6 owing to the successful doping and gating of CNT-FETs. According to our knowledge, our microfabricated hybrid devices attained the best-in-class responsivity in low-intensity visible-light detection. The extremely high sensitivity of the present $MAPbI_3$NW/CNT field-effect phototransistors (FEpT) is related to the photodoping of the carbon structure by photoexcited carriers of $MAPbI_3$NWs, a mechanism reported on graphene/$MAPbI_3$ hybrid photodetectors as well.[15–17] Importantly, however, because of the unipolar nature of CNT FETs, the present $MAPbI_3$NW/CNT FEpT photodetectors can be switched off unlike their graphene/$MAPbI_3$ counterparts.[15–17]

The fabricated field-effect transistors are appropriate tools to obtain valuable information about the light induced charge transfer phenomena at the interface by means of fairly simple electrical transport measurements, as FETs use an electric field to control the conductivity of a channel of one type of charge carrier in a semiconductor material. Detailed analysis of the device characteristics unraveled the charge transfer process between the intimate contact of $MAPbI_3$ and metallic or semiconducting CNTs. Despite the remarkable progress in prototype building, however, there is a lack of knowledge about the fundamental chemical and photo-physical characteristics of the interfaces formed between the carbon

[a]*Laboratory of Physics of Complex Matter (LPMC), Ecole Polytechnique Fédérale de Lausanne, 1015 Lausanne, Switzerland. E-mail: nafradi@yahoo.com*
[b]*Institute for Solid State Physics and Optics, Wigner Research Centre for Physics, Hungarian Academy of Sciences, 1525 Budapest, Hungary*

†Electronic supplementary information (ESI) available: Infrared and Raman spectroscopy with additional electronic transfer characterization. See DOI: 10.1039/c5nr06727h

nanomaterials and the organometal halide perovskites. Infrared (IR) and Raman spectroscopy of semitransparent highly purified single-walled nanotube buckypapers and $MAPbI_3$ nanowire composites confirmed the observed photo-induced charge transfer process.

Results and discussion

The fabrication of our $MAPbI_3$NW/CNT photo-FET started with the fabrication of an individual CNT based FET. The fabrication of CNT-FETs begins with metal catalyst deposition onto lithographically predefined positions. The cobalt-containing resist was spin-coated on a highly p-doped Si substrate with 200 nm thick SiO_2 thermally grown on top. Patterning the resist by electron-beam lithography created dots of the metal ion doped resist as small as 100 nm (Fig. 1a). The catalytic nanoparticles were formed by burning the organic resist at 800 °C in oxygen (Fig. 1b). Carbon nanotubes were grown by CVD at 800 °C using ethanol as a carbon source (Fig. 1c and S7†). Next, CNT-FETs were fabricated by patterning and evaporating the source and drain metal contacts (Ti/Pd 1 nm/70 nm, Fig. 1d).

The CNT-FET (Fig. 2a) was sensitized with a network of photoactive $MAPbI_3$ nanowires, deposited by the recently developed slip-coating method[18] (Fig. 2b). The hybrid device was subsequently covered with a 500 nm-thick polymethyl methacrylate (PMMA) layer to protect the organometal network from the detrimental effect of humidity.

In the pristine CNT-FET the high work function of the Pd contacts[19] and the p-type doping induced by the exposure to air (O_2)[20,21] led to dark transfer characteristics showing unipolar p-type behavior with a threshold voltage $V_{th} \approx 2$ V and 8.2×10^4 cm^2 V^{-1} s^{-1} mobility (Fig. 2c). The $MAPbI_3$ nanowire deposition caused both a shift of $V_{th} \approx -1$ V and a decrease of the CNT charge mobility by about 40% to 4.9×10^4 cm^2 V^{-1} s^{-1} (Fig. 2c).

The central finding of our paper is the remarkable photosensitivity of the hybrid $MAPbI_3$NW/CNT-FEpTs with responsivity $R = 7.7 \times 10^5$ A W^{-1} under low light conditions. The

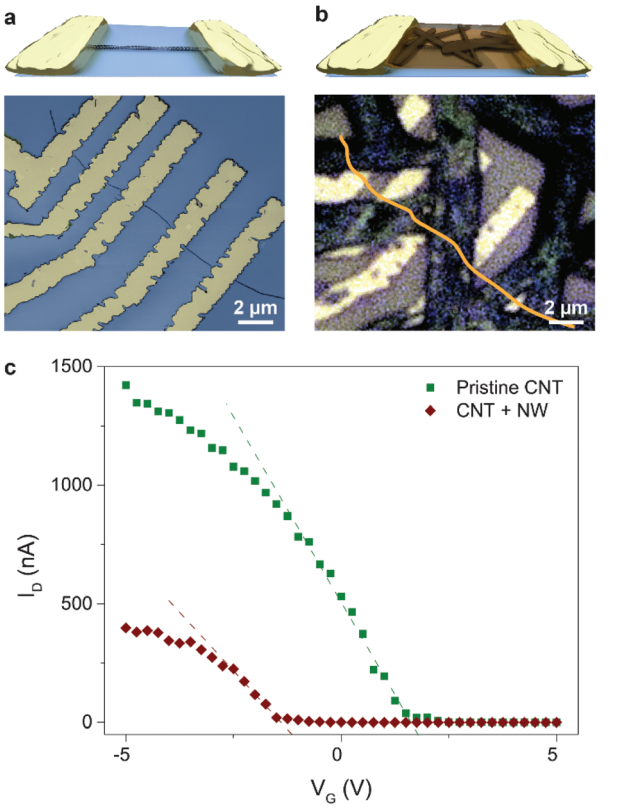

Fig. 2 (a) Schematic representation and false color SEM micrograph of a series of a representative CNT-FETs. (b) Schematic representation and optical micrograph of a representative $MAPbI_3$NW/CNT-FEpT. (c) Transfer characteristic of a representative device before (green curve) and after (red curve) sensitization (V_D = 0.2 V) in the dark. Dashed lines show the shift of the on–off threshold voltage V_{th}, and the reduction of the CNT mobility upon $MAPbI_3$ deposition.

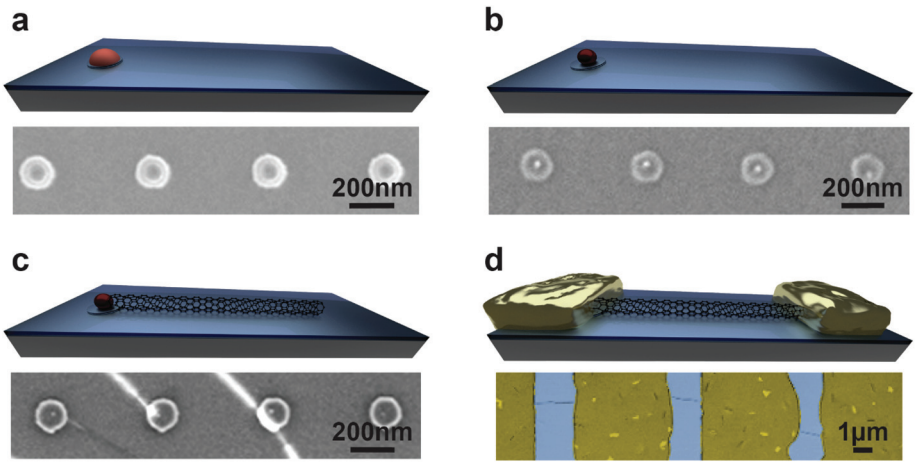

Fig. 1 Schematic representation and corresponding false-color high-resolution SEM micrographs of the process used for synthesizing the CNTs. (a) e-Beam lithography patterning of the metal-doped negative-tone resist. (b) Catalyst nanoparticle formation by thermal oxidation. (c) CNT synthesis by ethanol-assisted CVD. (d) Metal contact deposition by e-beam evaporation.

photoresponsivity of the hybrid device with illumination was tested with a red laser (λ = 633 nm) in the 62.5 nW mm^{-2} to 2.5 mW mm^{-2} intensity range.

Under illumination, electron–hole pairs are generated in $MAPbI_3$ nanowires. The holes are injected into the nanotube due to the chemical potential mismatch,[14] contributing to an increase in the output current in both the ON- and OFF-state of the $MAPbI_3$NW/CNT-FEpTs.

Above the threshold voltage, in the OFF-state of the $MAPbI_3$NW/CNT-FEpTs, the photocurrent, hence the total current, I_D, of the hybrid device, increases by increasing the incident irradiation power (Fig. 3b and S1†). The I_D current in the OFF-state does not show gate voltage (V_G) dependence, thus it corresponds to the intrinsic photocurrent generation of the $MAPbI_3$ nanowire network shortcutting the source–drain contacts, as was reported in our previous work.[18]

The evolution of the ON-state I_D current as a function of illumination intensity and V_G shows a markedly different behavior compared to the OFF-state (Fig. 3 and S1 and S2†). I_D-ON shows strong V_G dependence testifying that its origin is predominantly a CNT conduction channel. More interestingly, however, it shows a non-monotonous dependence on illumination intensity (Fig. 3 and S1 and S2†). Under low light conditions below 100 nW mm^{-2} intensity I_D increases monotonically by about a factor 2 relative to the dark current. By further increasing the light power, however, I_D rapidly falls and reaches I_D values observed for the OFF-state (Fig. S1 and S2†). Illuminating the device with light intensities higher than 95 μW mm^{-2} resulted in a complete switch-off of the nanotube channel conductance over the whole range of positive and negative gate biases applied (Fig. 3 and S1†). At the same time, V_{th} was independent of the light intensity.

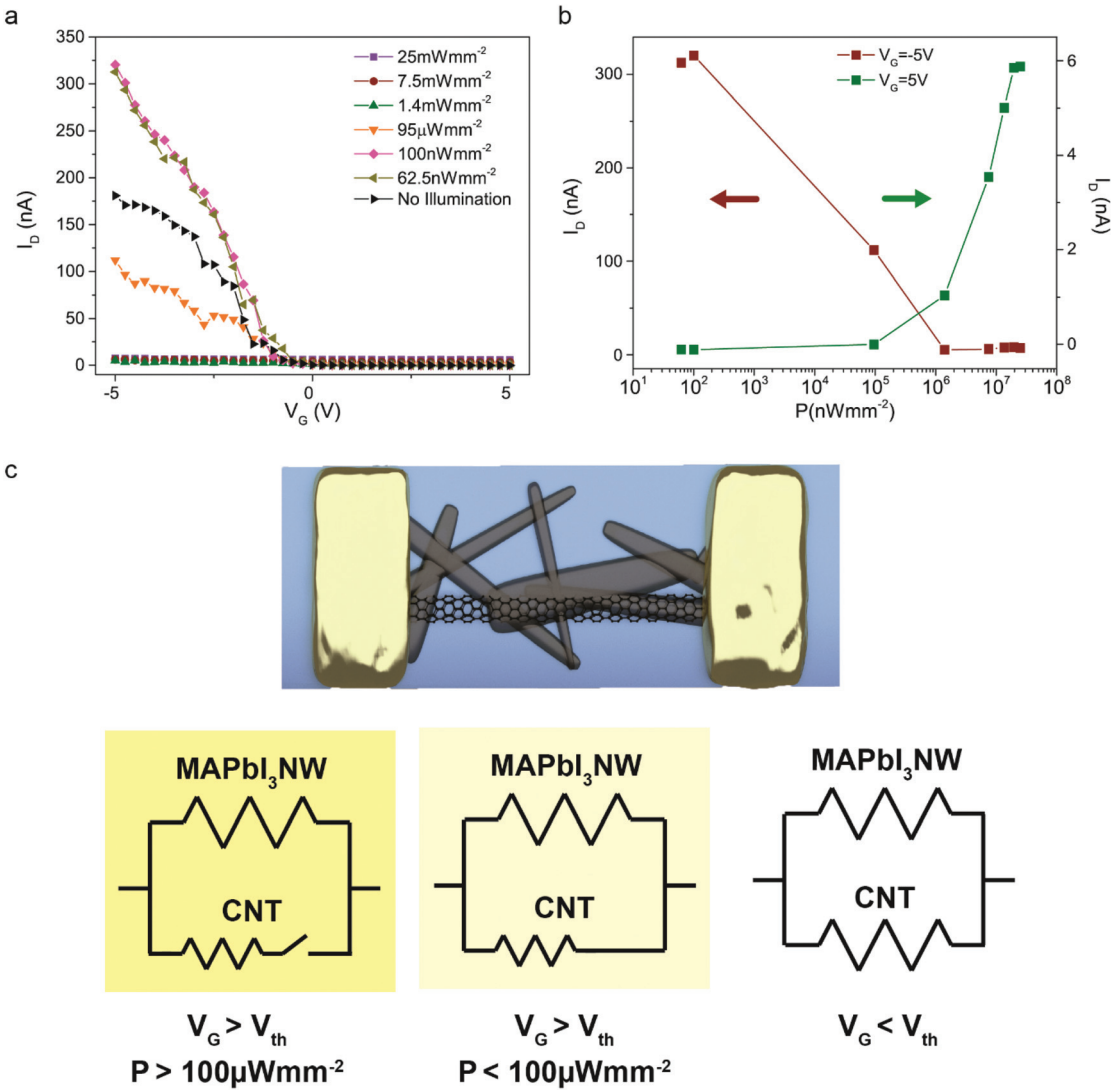

Fig. 3 (a) Transfer characteristic of the hybrid phototransistor upon different light irradiation intensities. (b) I_D at V_G = 5 and −5 V as a function of light power. (c) Schematic representation of the proposed two-parallel-resistor model used to describe our system.

The responsivity (R), the magnitude of the electrical signal output in response to a given light power, is one of the most important performance parameters of a photodetector. For the calculation of R the active area of the photodetector is needed. In order to conservatively estimate R of our device, we considered an active area equal to the distance between the contacts (3 μm) multiplied by the carrier diffusion length of photogenerated charge carriers in $MAPbI_3$ reported in the literature (*i.e.* ~1 μm).[22,23] In the ON-state (V_G = −5 V) and at extremely low light intensities (6.25 nW mm^{-2}–375 fW) responsivity as high as 7.7 × 10^5 A W^{-1} with an external quantum efficiency of 1.5 × 10^8% was measured (Fig. 4a). It is worth noting that the responsivities of the substituent CNT-FET and $MAPbI_3$NWs are 1 × 10^{-4} A W^{-1} (Fig. S9†) and 5 × 10^{-3} A W^{-1} (ref. 18) respectively. The synergy of these two nanomaterials brings about an eight orders of magnitude increase in responsivity. To the best of our knowledge this outperforms by about 7 orders of magnitude the best carbon-nanotube based photodetectors reported so far.[4] Moreover, the device gain is highly linear as a function of both V_D (Fig. 4a inset and S8†) and V_G (Fig. 4b) further facilitating applications.

The responsivity in accordance with the device characteristics presented in Fig. 3a rapidly drops by increasing the light power and reaches zero when the $MAPbI_3$NW/CNT-FEpTs reaches the light-induced OFF state.

Apart from responsivity, the other important benchmark of photodetector performance is the response time. For the hybrid device the response time to illumination is less than 1 s, (limited by the time resolution of our measurement setup) under all operating conditions tested (Fig. 4). On the other hand, the fall-time lasts between ~15 s (P < 95 μW mm^{-2}) and ~35 s (P > 95 μW mm^{-2}).

The photodiode characteristics of the individual CNT based $MAPbI_3$NW/CNT-FEpTs give valuable insight into the interface behavior of CNT and $MAPbI_3$NWs. Complications due to the intricate internal behavior of CNT films do not mask intrinsic interface properties, as we use single CNT devices. Moreover, metallic and semiconducting CNTs can be tested separately. In the case of $MAPbI_3$NW/CNTs, hybrid devices fabricated from metallic carbon nanotubes, the devices showed metallic behavior. Schottky barrier formation was not observed (Fig. S2†). For semiconducting CNT/$MAPbI_3$ devices the observed shift of V_{th} and the drop of CNT mobility (Fig. 2) upon the exposure of CNT-FETs to the concentrated $MAPbI_3$-DMF (dimethylformamide) solution indicate changes of the CNT chemical potential and increased effective disorder along the tubes, respectively.

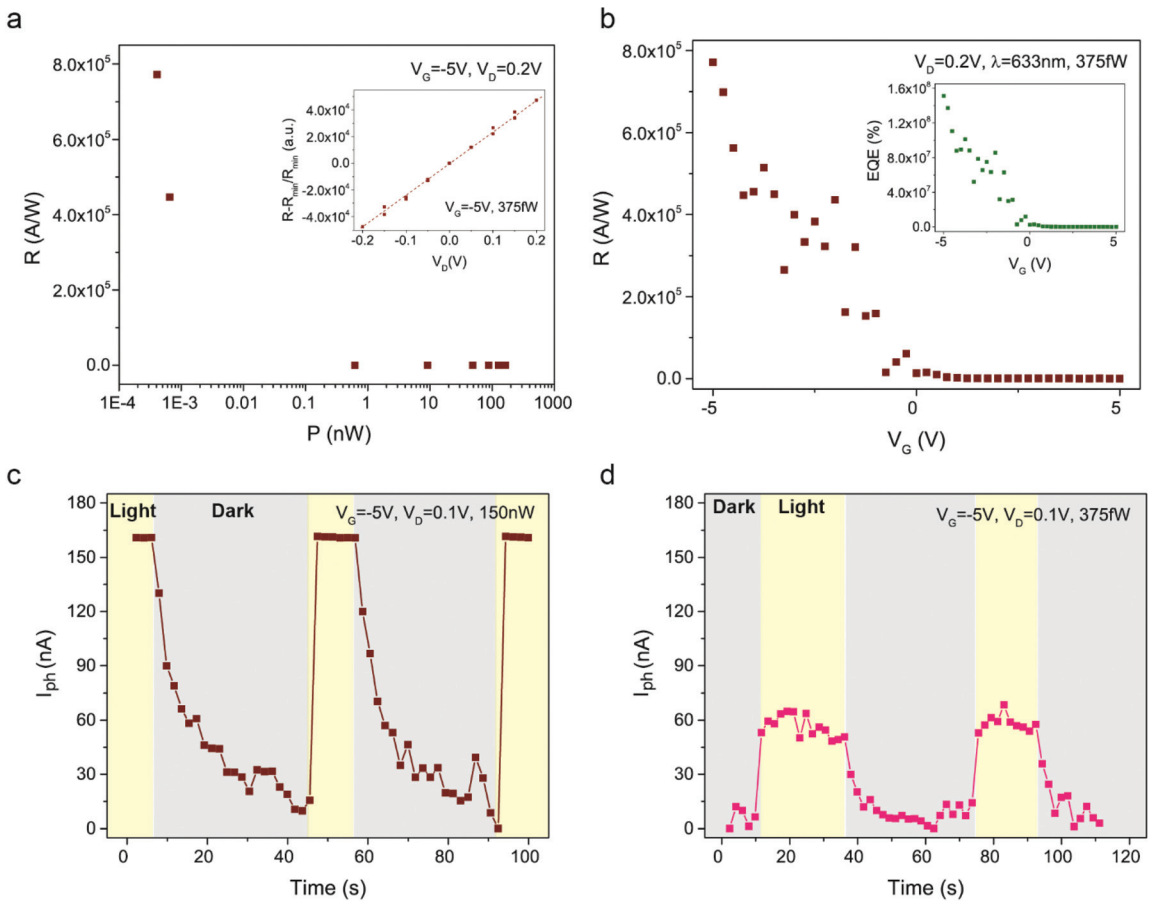

Fig. 4 (a) Responsivity of the hybrid device as a function of the light intensity and source-to-drain voltage (inset). (b) Responsivity and external quantum efficiency under different gate biases. (c and d) Response time under high, 150 nW, (left) and low, 375 fW, (right) light intensity.

In order to reveal the potential corrosive effects of the $MAPbI_3$-DMF solution on carbon nanotubes, a free-standing semi-transparent film enriched in semiconducting single walled CNTs was prepared and used as a 3D scaffold for the growth of $MAPbI_3$ nanowires (Fig. S3–S5†). We studied the interaction of the $MAPbI_3$ nanowires with the CNTs with and without illumination (633 nm LED source) by infrared, near-infrared and Raman spectroscopy. Depositing the nanowires affected only the IR, but not the Raman spectra of the CNT films (see ESI Fig. S3–S5†). We conclude by spectroscopic methods, that under illumination no other significant reaction can be detected between the nanowires and the nanotubes but charge transfer, resulting in mobile carriers. It should be noted, however, that the current running through a functional device can induce ion migration or additional electrochemical redox reactions at the carbon nanotube–$MAPbI_3$NW interface which can increase the number of defects, and hence reduce mobility, thus further optical measurements under operating conditions need to be done to clarify the origin of the mobility drop.

The photodiode characteristics of our $MAPbI_3$NW/CNT-FEpTs can be described by a parallel resistor model (Fig. 3b). When the hybrid CNT-FET is electrostatically switched off, the resistance of both 1D nanostructures (CNTs and $MAPbI_3$NWs) are in the GΩ range, and the current is low. Due to the closed conduction channel of the CNT, the photocurrent is essentially equal to the photo-generated charges in the $MAPbI_3$ nanowires. If the CNT-FET is in the ON regime due to electrostatic gating, its high conductivity dominates the performance of the hybrid device. Upon illumination the photogenerated positive charges enter the CNT and act as chemical doping, in agreement with IR and Raman spectroscopy. The photo-doping, however, does not shift the chemical potential of the CNTs indicating a nearby Van Hove singularity. The photo-induced negative charges, which are not injected in the CNT due to the work function mismatch,[14] constitute scattering centers inhomogeneously distributed along the carbon nanotube. The resulting random potential reduces the charge carrier mobility, thus the overall current. These two effects compete and at high light intensities the detrimental effects of the random potential overcompensate the doping and switch off the CNT conduction channel. Thus the $MAPbI_3$NW/CNT-FEpT acts as a light switch at high powers.

Conclusion

In conclusion, we demonstrated the gate voltage-dependent visible light photo-response of microfabricated individual $MAPbI_3$NW/CNT photo-FETs for the first time. In the mW mm^{-2} power range light soaking resulted in quenching the conductance of the ON-state p-channel of the individual CNT-FETs, effectively making the device an optical switch. The exposure of these hybrid devices to sub nW mm^{-2} light intensities, however, manifested a strong positive photocurrent. The best devices showed as high as 7.7×10^5 A W^{-1} responsivity and external quantum efficiencies of 1.5×10^8%, indicating that the device can be used as a low-intensity visible-light detector. We attributed this unconventional photocurrent transfer to be characteristic of the unique charge distribution over the 1D semiconductor nanotubes. Analysis of the gate dependent transfer characteristics in the dark and under illumination allowed the underlying photon induced charge transfer mechanisms between $MAPbI_3$ and metallic and semiconductor CNTs to be probed. The results have important implications in the fundamental understanding of the photophysical picture of $MAPbI_3$ and CNT interfaces and in the development and fabrication of organometallic halide perovskite based optoelectronic devices such as solar cells, LEDs, photodetectors, single photon-detectors and optical switches.

Experimental section

Resist preparation

A high-resolution cobalt-containing negative-tone resist was prepared by dissolving 0.2 wt% of 4-methyl-1-acetoxycalix[6]-arene (Synchem OHG) in monochlorobenzene and 0.2 wt% of Co(III) acetylacetonate, (Sigma-Aldrich GmbH, 99%). After stirring for 1 hour at 700 rpm the solution was filtered through a 0.2 mm Teflon membrane to remove potential solid residues.

Nanoparticle localization

The resist was patterned by e-beam lithography with a Vistec EBPG5000 operating at 100 kV and 1 nA. The nucleation centers were localized by a reactive ion etch step of 10 seconds with an Adixen AMS200 and a gas mixture of Ar and C_4F_8.

Carbon nanotube synthesis

The deposited nanoparticles are catalytically activated by a 10 min reduction at 800 °C under a controlled atmosphere (Ar/H_2 8 : 1 vol%). Next, ethanol vapor was introduced in the quartz tube using argon and hydrogen (1 : 2 vol%) as carrier gases. After 5 minutes the carbon source was evacuated and the samples were cooled down to room temperature.

Carbon nanotube film synthesis

Films of single walled carbon nanotubes were prepared from P2 and semiconductor enriched nanotubes as described by Wu *et al.*[24]

$MAPbI_3$ nanowire synthesis

The network of $MAPbI_3$ nanowires was subsequently deposited by the slip-coating technique reported by Horváth *et al.*[18]

Photoelectrical characterization

The photoelectric response measurements of the fabricated hybrid devices were performed using a standard DC technique. The light sources used were a red laser beam (λ = 633 nm) with a spot size of about 4 mm. All the measurements were performed at room temperature and in an ambient environment.

High-resolution scanning electron microscopy (SEM)

High-resolution scanning electron microscopy (SEM) was performed with a MERLIN Zeiss electron microscope.

Conflict of interest

The authors declare no competing financial interest.

Acknowledgements

This work was partially supported by the Swiss National Science Foundation (Grant No. 200021_144419 and 200021_160169) and the ERC advanced grant "PICOPROP" (Grant No. 670918). The work in Budapest was supported by the Hungarian National Research Fund (OTKA) no. 105691.

References

1 L. Yang, S. Wang, Q. Zeng, Z. Zhang and L.-M. Peng, Carbon Nanotube Photoelectronic and Photovoltaic Devices and their Applications in Infrared Detection, *Small*, 2013, **9**, 1225–1236, DOI: 10.1002/smll.201203151.

2 J. U. Lee, Photovoltaic effect in ideal carbon nanotube diodes, *Appl. Phys. Lett.*, 2005, **87**, 073101, DOI: 10.1063/1.2010598.

3 Y. H. Ahn, A. W. Tsen, B. Kim, Y. W. Park and J. Park, Photocurrent Imaging of p–n Junctions in Ambipolar Carbon Nanotube Transistors, *Nano Lett.*, 2007, **7**, 3320–3323, DOI: 10.1021/nl071536m.

4 M. Freitag, Y. Martin, J. A. Misewich, R. Martel and P. Avouris, Photoconductivity of Single Carbon Nanotubes, *Nano Lett.*, 2003, **3**, 1067–1071, DOI: 10.1021/nl034313e.

5 K. Balasubramanian, M. Burghard, K. Kern, M. Scolari and A. Mews, Photocurrent Imaging of Charge Transport Barriers in Carbon Nanotube Devices, *Nano Lett.*, 2005, **5**, 507–510, DOI: 10.1021/nl050053k.

6 V. Perebeinos, J. Tersoff and P. Avouris, Scaling of Excitons in Carbon Nanotubes, *Phys. Rev. Lett.*, 2004, **92**, 257402.

7 J. Even, *et al.*, Solid-State Physics Perspective on Hybrid Perovskite Semiconductors, *J. Phys. Chem. C*, 2015, **119**, 10161–10177, DOI: 10.1021/acs.jpcc.5b00695.

8 M. A. Green, A. Ho-Baillie and H. J. Snaith, The emergence of perovskite solar cells, *Nat. Photonics*, 2014, **8**, 506–514, DOI: 10.1038/nphoton.2014.134.

9 X. Mettan, *et al.*, Tuning of the Thermoelectric Figure of Merit of $CH_3NH_3MI_3$ (M=Pb,Sn) Photovoltaic Perovskites, *J. Phys. Chem. C*, 2015, **119**(21), 11506–11510, DOI: 10.1021/acs.jpcc.5b03939.

10 A. Pisoni, *et al.*, Ultra-Low Thermal Conductivity in Organic–Inorganic Hybrid Perovskite $CH_3NH_3PbI_3$, *J. Phys. Chem. Lett.*, 2014, **5**, 2488–2492, DOI: 10.1021/jz5012109.

11 J.-Y. Jeng, *et al.*, $CH_3NH_3PbI_3$ Perovskite/Fullerene Planar-Heterojunction Hybrid Solar Cells, *Adv. Mater.*, 2013, **25**, 3727–3732, DOI: 10.1002/adma.201301327.

12 Y. Shao, Z. Xiao, C. Bi, Y. Yuan and J. Huang, Origin and elimination of photocurrent hysteresis by fullerene passivation in $CH_3NH_3PbI_3$ planar heterojunction solar cells, *Nat. Commun.*, 2014, **5**, 5784, DOI: 10.1038/ncomms6784.

13 P. You, Z. Liu, Q. Tai, S. Liu and F. Yan, Efficient Semitransparent Perovskite Solar Cells with Graphene Electrodes, *Adv. Mater.*, 2015, **27**(24), 3632–3638, DOI: 10.1002/adma.201501145.

14 Z. Li, *et al.*, Laminated Carbon Nanotube Networks for Metal Electrode-Free Efficient Perovskite Solar Cells, *ACS Nano*, 2014, **8**, 6797–6804, DOI: 10.1021/nn501096h.

15 Y. Lee, *et al.*, High-Performance Perovskite–Graphene Hybrid Photodetector, *Adv. Mater.*, 2015, **27**, 41–46, DOI: 10.1002/adma.201402271.

16 M. Spina, *et al.*, Micro-engineered $CH_3NH_3PbI_3$ nanowire/graphene phototransistor for low intensity light detection at room temperature, *Small*, 2015, **11**(37), 4824–4828, DOI: 10.1002/smll.201501257.

17 M. He, *et al.*, Chemical decoration of $CH_3NH_3PbI_3$ perovskites with graphene oxides for photodetector applications, *Chem. Commun.*, 2015, **51**, 9659–9661, DOI: 10.1039/C5CC02282G.

18 E. Horváth, *et al.*, Nanowires of Methylammonium Lead Iodide ($CH_3NH_3PbI_3$) Prepared by Low Temperature Solution-Mediated Crystallization, *Nano Lett.*, 2014, **14**, 6761–6766, DOI: 10.1021/nl5020684.

19 Z. H. Chen, J. Appenzeller, J. Knoch, Y. M. Lin and P. Avouris, The role of metal-nanotube contact in the performance of carbon nanotube field-effect transistors, *Nano Lett.*, 2005, **5**, 1497–1502, DOI: 10.1021/Nl0508624.

20 K. Donghun, P. Noejung, K. Ju-hye, B. Eunju and P. Wanjun, Oxygen-induced p-type doping of a long individual single-walled carbon nanotube, *Nanotechnology*, 2005, **16**, 1048.

21 S. Heinze, *et al.*, Carbon Nanotubes as Schottky Barrier Transistors, *Phys. Rev. Lett.*, 2002, **89**, 106801.

22 S. D. Stranks, *et al.*, Electron-Hole Diffusion Lengths Exceeding 1 Micrometer in an Organometal Trihalide Perovskite Absorber, *Science*, 2013, **342**, 341–344, DOI: 10.1126/science.1243982.

23 G. Xing, *et al.*, Long-Range Balanced Electron- and Hole-Transport Lengths in Organic-Inorganic $CH_3NH_3PbI_3$, *Science*, 2013, **342**, 344–347, DOI: 10.1126/science.1243167.

24 Z. C. Wu, Z. H. Chen, X. Du, J. M. Logan, J. Sippel, M. Nikolou, K. Kamarás, J. R. Reynolds, D. B. Tanner, A. F. Hebard and A. G. Rinzler, Transparent, conductive carbon nanotube films, *Science*, 2004, **305**, 1273–1276.

